AIP | The Journal of Chemical Physics

The elusive S 2 state, the S 1/S 2 splitting, and the excimer states of the benzene dimer

Franziska A. Balmer, Maria A. Trachsel, Ad van der Avoird, and Samuel Leutwyler

Citation: The Journal of Chemical Physics **142**, 234306 (2015); doi: 10.1063/1.4922608
View online: http://dx.doi.org/10.1063/1.4922608
View Table of Contents: http://scitation.aip.org/content/aip/journal/jcp/142/23?ver=pdfcov
Published by the AIP Publishing

The elusive S_2 state, the S_1/S_2 splitting, and the excimer states of the benzene dimer

Franziska A. Balmer,[1] Maria A. Trachsel,[1] Ad van der Avoird,[2] and Samuel Leutwyler[1]
[1]*Department of Chemistry and Biochemistry, University of Bern, Freiestrasse 3, CH-3012 Bern, Switzerland*
[2]*Theoretical Chemistry, Institute for Molecules and Materials, Radboud University Nijmegen, Heyendaalseweg 135, 6525 AJ Nijmegen, The Netherlands*

(Received 7 February 2015; accepted 4 June 2015; published online 17 June 2015)

We observe the weak $S_0 \rightarrow S_2$ transitions of the T-shaped benzene dimers $(Bz)_2$ and $(Bz\text{-}d_6)_2$ about 250 cm^{-1} and 220 cm^{-1} above their respective $S_0 \rightarrow S_1$ electronic origins using two-color resonant two-photon ionization spectroscopy. Spin-component scaled (SCS) second-order approximate coupled-cluster (CC2) calculations predict that for the tipped T-shaped geometry, the $S_0 \rightarrow S_2$ electronic oscillator strength $f_{el}(S_2)$ is ~10 times smaller than $f_{el}(S_1)$ and the S_2 state lies ~240 cm^{-1} above S_1, in excellent agreement with experiment. The $S_0 \rightarrow S_1$ ($\pi\pi^*$) transition is mainly localized on the "stem" benzene, with a minor stem → cap charge-transfer contribution; the $S_0 \rightarrow S_2$ transition is mainly localized on the "cap" benzene. The orbitals, electronic oscillator strengths $f_{el}(S_1)$ and $f_{el}(S_2)$, and transition frequencies depend strongly on the tipping angle ω between the two Bz moieties. The SCS-CC2 calculated S_1 and S_2 excitation energies at different T-shaped, stacked-parallel and parallel-displaced stationary points of the $(Bz)_2$ ground-state surface allow to construct approximate S_1 and S_2 potential energy surfaces and reveal their relation to the "excimer" states at the stacked-parallel geometry. The $f_{el}(S_1)$ and $f_{el}(S_2)$ transition dipole moments at the C_{2v}-symmetric T-shape, parallel-displaced and stacked-parallel geometries are either zero or ~10 times smaller than at the tipped T-shaped geometry. This unusual property of the $S_0 \rightarrow S_1$ and $S_0 \rightarrow S_2$ transition-dipole moment surfaces of $(Bz)_2$ restricts its observation by electronic spectroscopy to the tipped and tilted T-shaped geometries; the other ground-state geometries are impossible or extremely difficult to observe. The $S_0 \rightarrow S_1/S_2$ spectra of $(Bz)_2$ are compared to those of imidazole · $(Bz)_2$, which has a rigid triangular structure with a tilted $(Bz)_2$ subunit. The $S_0 \rightarrow S_1/ S_2$ transitions of imidazole-(benzene)$_2$ lie at similar energies as those of $(Bz)_2$, confirming our assignment of the $(Bz)_2$ $S_0 \rightarrow S_2$ transition. © *2015 AIP Publishing LLC.* [http://dx.doi.org/10.1063/1.4922608]

I. INTRODUCTION

Molecular-beam electric-deflection measurements by Klemperer and co-workers in 1979 showed that the benzene dimer $(Bz)_2$ is polar, suggesting a T-shaped structure.[1] In 1993, Arunan and Gutowsky measured the rotational spectrum of supersonically cooled $(Bz)_2$ by Fourier-transform microwave spectroscopy; the rotational constant $B_0 = C_0$ is compatible with a T-shaped dimer with a distance of 4.94 Å between the centers-of-mass of the "stem" and "cap" Bz moieties.[2] The symmetric-top character of this spectrum[2] is surprising in that any *rigid* T-shaped $(Bz)_2$ structure must be an *asymmetric* top, see Figure 1. The microwave spectrum indeed exhibits multiple splittings that reflect rapid structural interconversion processes.[2] More recently, Szalewicz, van der Avoird, and their co-workers made great advances in the calculation of the intermolecular potential energy surface.[3,4] Upon incorporating a detailed permutation/inversion group-theoretical treatment of the *non-rigid* benzene dimer, they were able to predict the low-lying internal-rotation/tunneling states of $(Bz)_2$.[4] Schnell *et al.* recently re-measured and assigned the fine structure of the $(Bz)_2$ microwave spectrum in terms of vibration-rotation-tunneling (VRT) processes.[5–7]

The vibronic spectrum of supersonically cooled $(Bz)_2$ has been investigated since the 1980s using mass-selective resonant two-photon ionization (R2PI) spectroscopy.[8–20] These experiments identified the 0_0^0 band of the $(Bz)_2$ $S_0 \rightarrow S_1$ transition at 38 046 cm^{-1}, red-shifted by 40 cm^{-1} from the $S_0 \rightarrow S_1$ 0_0^0 band of Bz monomer at 38 086 cm^{-1}. The latter transition is strictly symmetry-forbidden as a one-photon electric-dipole transition,[21–23] so the question arises how the 0_0^0 (S_1) band of $(Bz)_2$ gains intensity. Smalley and co-workers already suggested "asymmetry in the crystal field" as a cause, i.e., that symmetry lowering of one or both of the Bz monomers renders the $S_0 \rightarrow S_1$ transition slightly allowed.[8] While the fluorescence quantum yield of $(Bz)_2$ is low, its ionization efficiency is high when compared to those of the $(Bz)_3$ and $(Bz)_4$ clusters produced in the same supersonic-jet expansion.[8,9,18] This was interpreted in terms of vertical excitation of $(Bz)_2$ into a T-shaped S_1 state local minimum, followed by rapid rearrangement to a stacked-parallel structure corresponding to the lowest excimer state of $^1B_{1g}$ symmetry.[8,9,18]

Since the two Bz monomers in $(Bz)_2$ should give rise to two transitions corresponding to the $S_0 \rightarrow S_1$ and the $S_0 \rightarrow S_2$ excitations of $(Bz)_2$, Schlag and co-workers subsequently

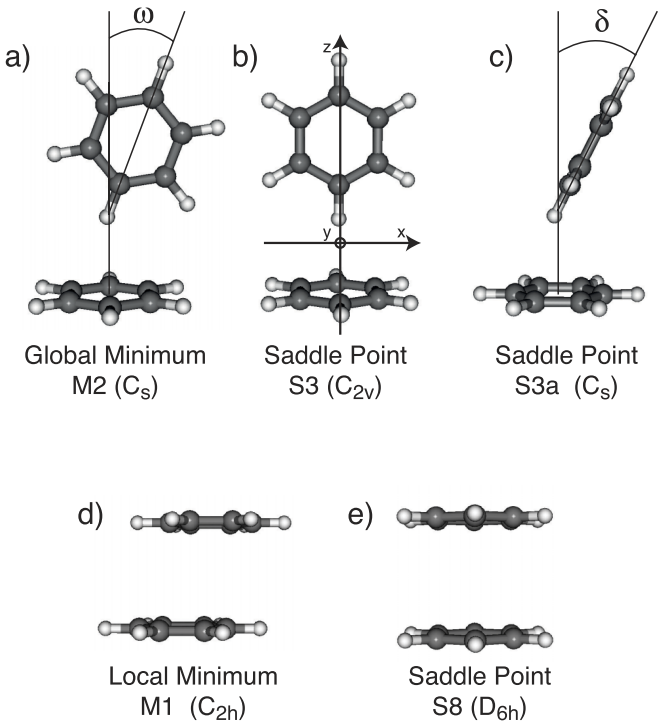

FIG. 1. Ground-state stationary-point structures of $(benzene)_2$: (a) the minimum-energy C_s-symmetric structure **M2** with definition of the tipping angle ω, (b) the C_{2v}-symmetric saddle-point **S3** with the inertial axis system, (c) the T-shaped C_s'-symmetric saddle point **S3a** with definition of the tilting angle δ, (d) the parallel-displaced C_{2h}-symmetric local minimum **M1**, and (e) the stacked-parallel D_{6h}-symmetric saddle point structure **S8**. The conformer nomenclature is defined in Refs. 3 and 4.

undertook detailed spectroscopic studies of $(Bz\text{-}h_6)_2$, the $(Bz\text{-}h_6)(Bz\text{-}d_6)$ heterodimer, the fully deuterated homodimer $(Bz\text{-}d_6)_2$, and of other D- and ^{13}C-isotopomers of $(Bz)_2$, attempting to determine the excitonic splitting between the $S_0 \rightarrow S_1$ and $S_0 \rightarrow S_2$ origins of $(Bz)_2$, as well as the excited-state structure of $(Bz)_2$.[10,12] Combining the spectroscopic results with early high-level *ab initio* calculations of $(Bz)_2$, Schlag, Hobza, and co-workers concluded that the $(Bz)_2$ structure is T-shaped,[10,12,24,25] in good agreement with the later microwave structure.[2] They interpreted a ~2 cm^{-1} splitting of the 0_0^0 band of $(Bz)_2$ as arising from the excitonic S_1/S_2 splitting.[10,12] Felker and co-workers performed stimulated-Raman spectroscopic measurements on $(Bz)_2$ and its isotopomers, determined that $(Bz)_2$ consists of two inequivalent monomers,[13–16] and interpreted the low-frequency intermolecular and intramolecular Raman vibrational bands in terms of a T-shaped dimer.[13–16] Erlekam *et al.* have recorded the IR spectrum of $(Bz)_2$[19] and observed the b_{1u} stretch frequency of the stem Bz moiety, in agreement with the T-shaped structure,[19,20] and the calculated C–H stretching frequency shift.[26]

Felker and co-workers pointed out that the symmetry of the stem-Bz in the T-shaped dimer is lowered from D_{6h} to C_{2v}, rendering the $S_0 \rightarrow S_1$ electronic origin weakly allowed, but that the internal rotation of the cap-Bz renders its site symmetry C_{6v}, in which the 0_0^0 band remains forbidden.[14–16] Nevertheless, $(Bz)_2$ has *two* excited states that correlate with the $S_0 \rightarrow S_1$ excitation of its two Bz constituents. Indeed, Henson *et al.* tentatively assigned a "6–8 cm^{-1} blue-shifted $1_1^0 6_0^1$ band" localized on the cap-Bz moiety.[14] As the calculations and experiments below will show, the separation between the S_1 and S_2 0_0^0 transitions of the T-shaped dimer is ~200 cm^{-1}. Also, it is dominated by the "site-splitting" energy[13–16] and not by the excitonic splitting.[10,12]

Because benzene lacks a dipole moment, the lowest-order electrostatic interaction in $(Bz)_2$ is the relatively weak quadrupole-quadrupole interaction, the major part of the binding coming from dispersive interactions, which require high-level correlated treatments. For this reason, Bz_2 and especially the relative energies of the T-shaped, tilted T-shaped, stacked-parallel, and parallel displaced geometries have been used as a benchmark system for high-level electronic structure calculations.[27–33] Szalewicz and co-workers, who calculated the six-dimensional intermolecular PES of Bz_2 using the symmetry-adapted perturbation theory (density functional theory) (SAPT(DFT)) method, located T-shaped and stacked minima as well as many index-1 saddle points.[3] They later complemented this work by performing CCSD(T): coupled-cluster with singles, doubles and perturbative triples excitations calculations at three minima and nine index-1 stationary points.[4] Below, we employ their nomenclature[3] for the stationary points **M2**, **S3**, **S3a**, **M1**, and **S8**, which are shown in Figure 1. Xantheas and co-workers have recently performed a complete basis set (CBS) study of the **M1** parallel-displaced dimer with the CCSD(T) method and obtained a CCSD(T)/CBS binding energy $D_e = -2.65 \pm 0.02$ kcal/mol.[33] This value is only 0.03 kcal/mol lower than the CCSD(T) $D_e = -2.62$ kcal/mol CCSD(T) value of Szalewicz and co-workers, which was not optimized for the intramolecular degrees of freedom.[4]

We first concentrate on the C_s-symmetric, tipped T-shaped global minimum **M2** and on the low-lying C_{2v}-symmetric index-1 saddle point **S3**, see Figure 1.[3,4] We address the properties of the S_1 and S_2 states of $(Bz)_2$ both spectroscopically and theoretically, with a focus on the S_2 state. We present vibronic spectra of $(Bz)_2$ and the $(Bz\text{-}d_6)_2$ isotopomer that show weak band systems starting ~240 cm^{-1} above the respective $S_0 \rightarrow S_1$ electronic origins. Using approximate second-order coupled-cluster CC2 calculations, we predict (1) the energetic order and the splitting between the S_1 and S_2 excited states, (2) the electronic transition dipole moments (TDMs) and their orientations, and (3) the interpretation of the respective electronic transitions in terms of orbital excitations on the stem and cap Bz moieties. In agreement with Felker *et al.*,[13–16] we find that the lowest electronic excitation of the cap-Bz—corresponding to the $(Bz)_2$ S_2 state—is extremely weak in the C_{2v}-symmetric T-shaped dimer **S3**. However, displacement along the ω tipping angle from **S3** towards the tipped T-shaped global minimum **M2** increases *both* the $f_{el}(S_1)$ and $f_{el}(S_2)$ oscillator strengths which correspond to the stem and cap electronic transitions. (We use "tipping" for consistency with our previous work[34–36] but note that the ω coordinate was denoted "tilt" in Refs. 4–7.) We also compare the vibronic spectrum of $(Bz)_2$ to the recently measured vibronic spectrum of the imidazole · $(Bz)_2$ cluster,[37] which has a triangular structure with the $(Bz)_2$ subunit bent more strongly than in $(Bz)_2$. In Sec. IV, we extend the SCS-CC2 calculations to the S_1 and S_2 states of two low-lying ground-state

saddle-point geometries **S3a**, **S8** and the parallel displaced local minimum **M1**,[3,4] see Figure 1.

II. METHODS

A. Computational methods

The S_1 excited state of Bz_2 has been characterized at several different levels of theory, including time-dependent DFT (TD-DFT),[27,29] complete active-space second-order perturbation theory (CASPT2),[28] linear-response coupled cluster methods [LR-CC2, LR-CCSD, and LR-CCSDR(3)],[30] and equation-of-motion CCSD,[31] but only at the stacked-parallel **S8** and parallel-displaced **M1** geometries. These structures transform as B_{1g} and B_g in the D_{6h} and C_{2h} point groups, respectively (see Figure 1), and correspond to the "excimer" geometry of Bz_2^*. However, the stacked **S8** geometry is not a ground-state minimum, and the **M1** structure is a local minimum that has not been experimentally detected in 25 years of research. On the other hand, the excited state tipped T-shaped minimum in the S_1 state has not been treated by the same high-level correlated methods that allow structure optimization and normal-mode frequency calculations.

In order to study the T-shaped Bz_2 minimum in the S_1 state, we employed the spin-component scaled (SCS) CC2 method with large and diffuse basis sets.[38–40] The SCS-CC2 method has a good cost/accuracy ratio. Benchmark studies by Hättig and co-workers employing five excited-state methods (TD-B3LYP, ADC(2), CC2, SCS-CC2, and SOS-CC2) on 66 different medium-sized and large aromatic organic molecules with 10-78 atoms comparing the calculated and experimental 0-0 transition energies have shown that the SCS-CC2 gives the best performance, even better than that of the CC2 method.[40] Spin component scaling not only improves the CC2 excited state energies but also the dipole moments and vibrational frequencies.[38–40]

We optimized the ground state of $(Bz)_2$ with the SCS variant of the second-order Moller-Plesset perturbation theory (MP2) method,[40–43] using the Dunning augmented correlation-consistent basis sets aug-cc-pVXZ with X = D, T, Q, which are abbreviated as aVXZ below. In the recent CCSD(T) study of Xantheas and co-workers on the parallel displaced Bz_2 dimer,[33] they also employed SCS-MP2 and obtained a "best estimate" binding energy $D_e = -2.65 \pm 0.02$ kcal/mol that is identical to the CCSD(T)/CBS D_e discussed above.[33] The SCS-CC2 vertical excitations to the S_1 and S_2 states were calculated at the respective SCS-MP2 ground-state equilibrium structures in the resolution of the identity (RI) approximation[43] employing the aVXZ basis sets. The like and unlike spin components of the MP2 and CC2 energies were scaled according to Grimme.[42] The SCS-MP2/aug-cc-pVTZ optimized Cartesian coordinates of the T-shaped **M2** minimum and the **S3** and **S3a** saddle point structures are given in Tables I–III of the supplementary material.[44]

All calculations were performed using Turbomole 6.3 (RICC2 module).[45] For this weakly bound complex, the standard Turbomole thresholds had to be lowered to the following non-standard values: SCF and one-electron density convergence, 10^{-9} au and 10^{-8} au, respectively. Geometry and force thresholds for structure optimizations were 10^{-8} au (energy change), 6×10^{-6} au (maximum displacement element), 10^{-6} au (maximum gradient element), 4×10^{-6} au (RMS displacement), and 10^{-6} au (RMS gradient).

B. Experimental methods

Benzene dimer $(Bz\text{-}h_6)_2$ and its isotopomer $(Bz\text{-}d_6)_2$ were produced and cooled in a pulsed supersonic jet expansion. The Bz (Fluka, 99%) or Bz-d_6 (Cambridge Isotopes, 99.5% isotopic purity) sample was held at −45 °C to −35 °C, corresponding to 1-2 mbar Bz pressure, and seeded into the neon carrier gas (Linde, ≥99.995%) at a backing pressure of 1.3 bar. For the imidazole · $(benzene)_2$ ($Im \cdot Bz_2$) measurements,[37] the imidazole (Sigma, ≥99.5%) was placed in the pulsed jet nozzle (0.4 mm diameter) and heated to 75–80 °C, corresponding to an imidazole pressure of 0.4-0.6 mbar.

Mass-selective two-color (2C) R2PI spectra of the Bz_2 dimers and $Im \cdot Bz_2$ trimer were recorded over the 37 500 –39 000 cm^{-1} range. Electronic excitation was performed with a frequency-doubled NarrowScan dye laser (Coumarin 307 in EtOH, ~200 μJ/pulse) pumped by the 355 nm output of a Nd:YAG laser. Ionization was induced by a second frequency-doubled dye laser (FL3002, Fluorescein 27 in basic MeOH, 1 mJ/pulse) at 275 nm. The ions were separated in a time-of-flight (TOF) mass spectrometer and detected by a double microchannel plate detector. As the $Im \cdot Bz_2$ cluster fragments into the $Im \cdot Bz^+$ mass channel, the true two-color R2PI spectrum of $Im \cdot Bz_2$ was obtained by IR/UV holeburning measurements. The IR laser pulse (~8 mJ) generated by a 10 Hz LaserVision OPO/OPA system (pumped by a Nd:YAG laser) was fixed at the NH-stretch of imidazole in the $Im \cdot Bz_2$ complex (3452 cm^{-1}). Two 2C-R2PI spectra were then measured successively in the $Im \cdot Bz^+$ mass channel, first without and then with previous depletion of the ground state.

III. RESULTS

A. Computational results

1. Vertical excitation energies

At the C_s-symmetric **M2** ground-state minimum geometry, the $S_0 \rightarrow S_1$ and $S_0 \rightarrow S_2$ vertical excitation energies calculated by the SCS-CC2 method are separated by 170 –260 cm^{-1}, corresponding to the site-splitting[13–15] between the stem and cap Bz molecules. The splitting is 262 cm^{-1} with the aVDZ, 250 cm^{-1} with the aVTZ, and 244 cm^{-1} with the aVQZ basis set, as is shown in Figure 2. At the C_{2v} (**S3**) geometry, the S_1/S_2 splitting is slightly smaller, about 200–210 cm^{-1} with the aVXZ basis sets. The irreps of the S_1 and S_2 states are A' in the C_s geometry; in the C_{2v} geometry, both excited states are B_1. The predictions of the aVXZ basis sets are in good mutual agreement, while the much smaller SVP basis set predicts ~50 – 100 cm^{-1} smaller splittings, as shown in Figure 2.

The expected S_1/S_2 site splitting of the T-shaped benzene dimer can be roughly estimated from previous spectroscopic experiments: the weakly allowed S_1 0_0^0 transition of the stem Bz is spectrally shifted by $\delta\nu = -44.4$ cm^{-1} relative to the

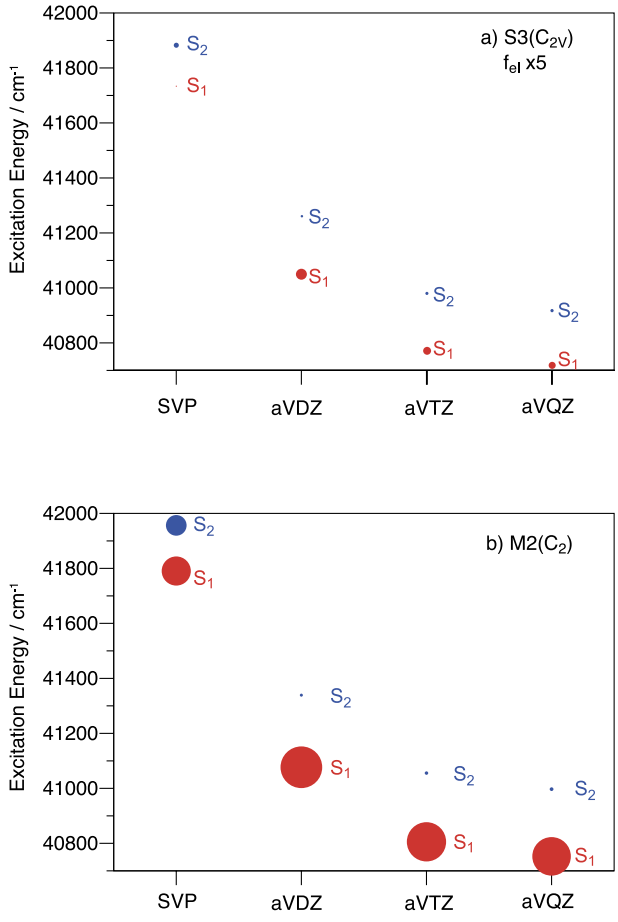

FIG. 2. SCS-CC2 vertical transition frequencies and oscillator strengths f_{el} for the $S_0 \rightarrow S_1$ (red dots) and $S_0 \rightarrow S_2$ transitions (blue dots) of the (a) **S3** and (b) **M2** conformers of $(benzene)_2$, as a function of basis set size. The relative size of $f_{el}(S_1)$ and $f_{el}(S_2)$ is indicated by the dot radii; these are enlarged 5× in (a) relative to (b).

(forbidden) electronic origin of bare Bz.[8–16,18] On the other hand, the spectral shift $\delta\nu$ of the cap-Bz transition can be estimated from the spectra of X–H $\cdots\pi$ bonded T-shaped Bz complexes such as Cl–H $\cdots$ Bz, $H_2O \cdots$ Bz, and $D_2O \cdots$ Bz, where the Bz is in the cap position.[46–49] The $S_0 \rightarrow S_1$ electronic origins of the cap-Bz become allowed due to the slight tilt of the X–H donor axis relative to the Bz surface normal and are typically shifted by $\delta\nu$ = +80 to +125 cm^{-1} above the Bz 0_0^0 band.[46–49] Combining the stem-type and cap-type spectral shifts yields a rough estimate for the site splitting of about 120–170 cm^{-1}, in qualitative agreement with the SCS-CC2 calculated values.

2. Electronic oscillator strengths

The SCS-CC2 calculated electronic oscillator strengths $f_{el}(S_1)$ and $f_{el}(S_2)$ depend both on the size of the basis set and geometry of the dimer. Figure 2(a) shows the calculated oscillator strengths at the C_{2v}-symmetric T-shaped **S3** geometry and Figure 2(b) shows the analogous results at the C_s-symmetric **M2** minimum. The $f_{el}(S_1)$ and $f_{el}(S_2)$ values are also listed in Table I.

With the diffuse aVXZ basis sets, $f_{el}(S_1)$ is about 10 times larger than $f_{el}(S_2)$ in both the C_{2v} and C_s geometries. With the smaller SVP basis set, $f_{el}(S_2)$ is larger than $f_{el}(S_1)$ in the **S3** geometry, while in the **M2** geometry, they are nearly equal, see Figures 2(a) and 2(b). While the SVP transition energies are reasonable, these electronic oscillator strengths are clearly less reliable, so they will be disregarded from now on. By contrast, the aVXZ electronic oscillator strengths change little with increasing basis set size, both at the C_{2v} and C_s geometries as can be seen in Figure 2. Both $f_{el}(S_1)$ and $f_{el}(S_2)$ are small, 10^{-5}–10^{-4}, as is expected for a nominally forbidden transition which becomes allowed via the slight distortion induced by the dimer formation. Note that $f_{el}(S_2)$ is *not* equal to zero, which suggests that the $S_0 \rightarrow S_2$ transition might be observable for the T-shaped dimer.

3. Orbital excitations

To facilitate the discussion, we discuss the molecular orbital (MO) excitations based on the aVDZ orbitals, which are more compact than the aVTZ and aVQZ ones. Figure 3 shows that for the **S3** structure, the $S_0 \rightarrow S_1$ transition consists of a stem-localized $\pi\pi^*$ transition (12.6%) with small contributions from cap-π orbitals, a stem-$\pi \rightarrow$ cap-π^* charge-transfer transition (12.5%), and a second stem-$\pi \rightarrow$ stem-π^* transition (12.5%) with no contribution from cap-π orbitals. For the **M2** structure, shown in Figure 4, the $S_0 \rightarrow S_1$ transition is dominated by a stem-$\pi \rightarrow$ cap-π^* charge-transfer transition. Note that in the **M2** geometry, the stem-π and cap-π orbitals are more strongly mixed than in the **S3** structure. For both structures, the $S_0 \rightarrow S_2$ transition is composed of two $\pi\pi^*$ excitations that are mainly located on the cap-Bz. The larger contribution (20.3%) also has a very small $\pi\pi^*$ transition on the stem-Bz, while the slightly weaker transition (19.3%) is entirely located on the cap moiety.

4. Transition dipole moments

Figure 5 shows the SCS-CC2 calculated TDM vectors of $(Bz)_2$ at the **M2** geometry, as a function of basis set size for the aVXZ (X = D, T, Q) basis sets; all three calculations were done at the SCS-MP2/aVTZ optimized geometry, see the supplementary material.[44] The $S_0 \rightarrow S_1$ and $S_0 \rightarrow S_2$ TDM vectors are both oriented within the σ_v symmetry plane of the dimer. The $S_0 \rightarrow S_1$ vector directions and lengths are similar for the three basis sets, lying at an angle of ~40° relative to the cap-Bz surface normal. The $S_0 \rightarrow S_2$ TDM vectors, which we have drawn at the center-of-mass of the cap Bz because they are associated with this moiety, do *not* lie within the cap-Bz plane, but are tipped (with the aVDZ basis set) or approximately normal to this plane (for the aVDZ and aVQZ basis sets).

A comparison of Figures 2(a) and 2(b) reveals that both $f_{el}(S_1)$ and $f_{el}(S_2)$ are considerably smaller at the **S3** than at the **M2** geometry. This implies that f_{el} is a function of the tipping angle ω, see Figure 1(a). In Figure 6, we show the SCS-CC2/aVTZ calculated oscillator strengths $f_{el}(S_1)$ and $f_{el}(S_2)$ calculated as a function of ω: both oscillator strengths indeed increase by ~10 times when ω is increased from 0° to 20°. Throughout the entire angle range shown, $f(S_1)$ is 5–10 times larger than $f_{el}(S_2)$. The strong dependence of $f_{el}(S_1)$ and $f_{el}(S_1)$

TABLE I. $(Benzene)_2$ oscillator strengths f_{el} and fractional orbital excitation contributions to the $S_0 \rightarrow S_1$ and $S_0 \rightarrow S_2$ transitions, calculated with the SCS-CC2/aVTZ method (and aVDZ for the oscillator strengths) at SCS-MP2/aVTZ ground state optimized structures.

	aug-cc-pVDZ	aug-cc-pVTZ		
Structure	f_{el}	f_{el}	Fraction	Assignment
S3/C_{2v}				
			12.6%	stem/cap $\pi \rightarrow$ stem π^*
$S_0 \rightarrow S_1$	6.43×10^{-6}	4.65×10^{-6}	12.5%	stem/cap $\pi \rightarrow$ cap/stem π^* charge transfer
			12.5%	stem $\pi \rightarrow$ stem π^*
$S_0 \rightarrow S_2$	1.44×10^{-6}	1.83×10^{-6}	24.6%	cap/stem $\pi \rightarrow$ cap/stem π^*
			22.4%	cap $\pi \rightarrow$ cap π^*
M2/C_s				
$S_0 \rightarrow S_1$	1.22×10^{-4}	1.15×10^{-4}	12.7%	stem/cap $\pi \rightarrow$ cap/stem π^* charge transfer
$S_0 \rightarrow S_2$	8.98×10^{-6}	1.02×10^{-5}	20.3%	cap/stem $\pi \rightarrow$ cap/stem π^*
			19.2%	cap $\pi \rightarrow$ cap π^*
S3a/C_s				
$S_0 \rightarrow S_1$	4.39×10^{-6}	3.52×10^{-6}	10.3%	stem/cap $\pi \rightarrow$ stem/cap π^*
$S_0 \rightarrow S_2$	1.58×10^{-5}	1.44×10^{-5}	27.3%	cap/stem $\pi \rightarrow$ cap/stem π^*
M1/C_{2h}				
$S_0 \rightarrow S_1$	0.0	0.0	64.6%	$\pi \rightarrow \pi^*$ delocalized by symmetry
$S_0 \rightarrow S_2$	1.57×10^{-6}	3.50×10^{-6}	66.3%	$\pi \rightarrow \pi^*$ delocalized by symmetry
S8/D_{6h}				
$S_0 \rightarrow S_1$	0.0	0.0	28.9%	$\pi \rightarrow \pi^*$ delocalized by symmetry
$S_0 \rightarrow S_2$	0.0	0.0	20.7%	$\pi \rightarrow \pi^*$ delocalized by symmetry

on the intermolecular vibrational ω coordinate implies that there is a coordinate-dependent contribution for ω_0^n vibronic transitions. The vibronic transition dipole moments to levels with high $\langle\omega\rangle$ acquire intensity beyond the purely electronic transition dipole moment, equivalent to a large Herzberg-Teller effect.

At this point, we note that the tipped T-shaped structure **M2** does *not* correspond to a vibrational eigenstate. The correct $v = 0^+/0^-$ eigenstates in both the ground and excited electronic states are the + and − combinations of localized wave functions in the two wells that correspond to the "left" and "right" localized minima (where Figure 1(a) shows the right-localized minimum). In the vibrational-electronic picture, the

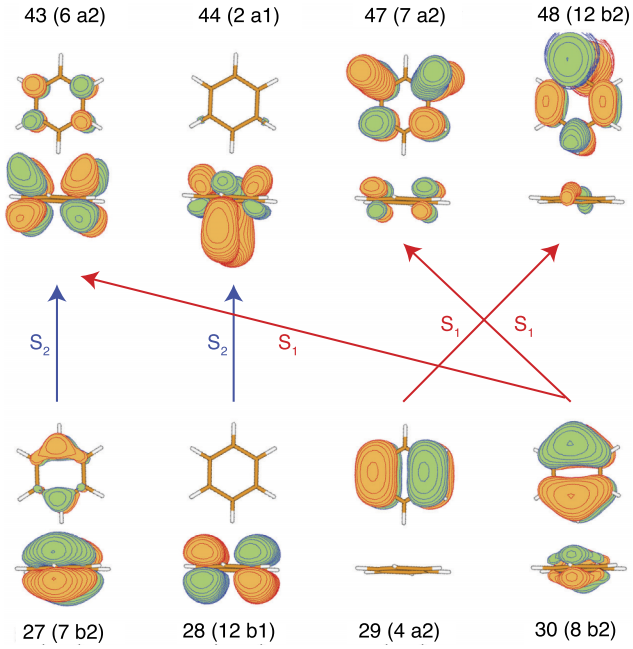

FIG. 3. Dominant orbital excitation contributions to the $S_0 \rightarrow S_1$ (red) and $S_0 \rightarrow S_2$ transitions (blue) of the C_{2v}-symmetric **S3** structure of $(benzene)_2$ (SCS-CC2/aug-cc-pVDZ calculation).

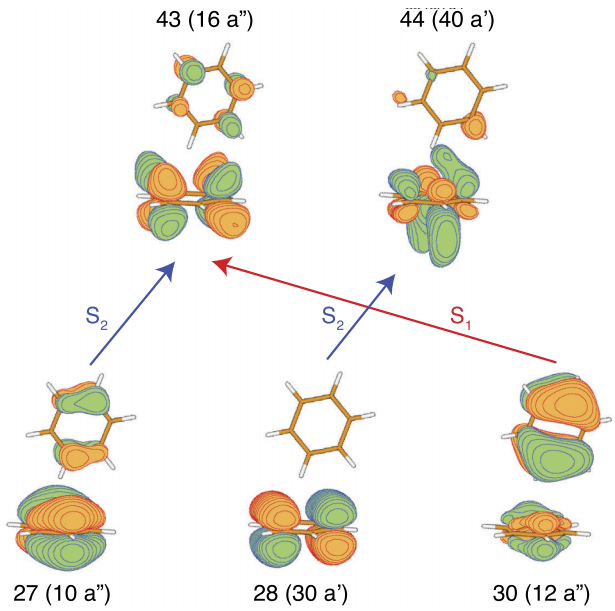

FIG. 4. Dominant orbital excitations corresponding to the $S_0 \rightarrow S_1$ (red) and $S_0 \rightarrow S_2$ transitions (blue) for the C_s-symmetric **M2** structure of $(benzene)_2$ (SCS-CC2/aug-cc-pVDZ).

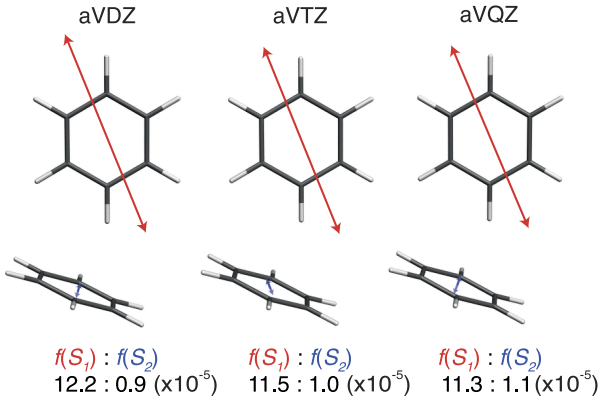

FIG. 5. SCS-CC2 transition dipole moments of the $S_0 \rightarrow S_1$ (red) and $S_0 \rightarrow S_2$ (blue) transitions of the **M2** (C_s) structure of $(Bz)_2$, as a function of basis set size from aVDZ to aVQZ.

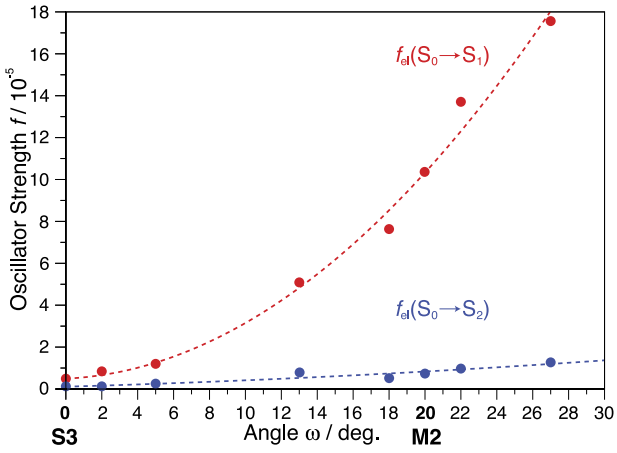

FIG. 6. SCS-CC2/aVTZ calculated oscillator strengths $f_{el}(S_1)$ (in red) and $f_{el}(S_2)$ (in blue) of the T-shaped C_s-symmetric $(benzene)_2$ conformer, as a function of the tipping angle ω. The f_{el} values are calculated at displacements along the S_0 state ω normal-mode eigenvectors of the **S3** and **M2** structures, whose respective ω_e angles 0° and 20° are indicated.

reason that the $S_0 \rightarrow S_2$ transition of $(Bz)_2$ becomes allowed is not due to symmetry-lowering or -breaking, but because it is accompanied by $v'' = 0^+ \rightarrow v' = 0^-$ or $v'' = 0^- \rightarrow v' = 0^+$ transitions between the tunneling states. These wave functions have vanishing amplitudes as the $(Bz)_2$ geometry approaches the **S3** geometry.

B. Resonant two-photon ionization spectra

Figure 7 shows the 2C-R2PI spectra of $(Bz\text{-}h_6)_2$ and $(Bz\text{-}d_6)_2$. The electronic origin of $(Bz\text{-}h_6)_2$ lies at 38 041.7 cm^{-1} and that of $(Bz\text{-}d_6)_2$ at 38 242.9 cm^{-1}, in agreement with the previous work.[12–16,19] About 240 cm^{-1} above the $S_0 \rightarrow S_1$ electronic origin, a series of weak bands is observed for both $(Bz\text{-}h_6)_2$ and $(Bz\text{-}d_6)_2$. In the $(Bz\text{-}h_6)_2$ spectrum, Figure 7(a), the first of these bands lies at +238 cm^{-1}; it is especially noticeable in the 10× magnified spectrum. In the benzene monomer S_1 (B_{2u}) state, the low-frequency ν'_{16} out-of-plane deformation mode has been inferred to lie at +237.5 cm^{-1}.[23] Note, however, that this out-of-plane vibration is symmetry-forbidden in the $S_0 \rightarrow S_1$ spectrum of Bz-h_6. In the $(Bz\text{-}d_6)_2$ spectrum, Figure 7(b), the lowest of the weak bands is observed at +208.5 cm^{-1}, in very good agreement with the $\nu'_{16} = 208\ cm^{-1}$ frequency of S_1 state C_6D_6.[50] Thus, the $(Bz\text{-}h_6)_2$ and $(Bz\text{-}d_6)_2$ spectra in Figures 7(a) and 7(b) are consistent in showing a 16^1_0 excitation of the stem Bz moiety.

Since Bz-h_6 and Bz-d_6 have *no* other low-frequency vibrations in the 200-300 cm^{-1} range, we assign the following

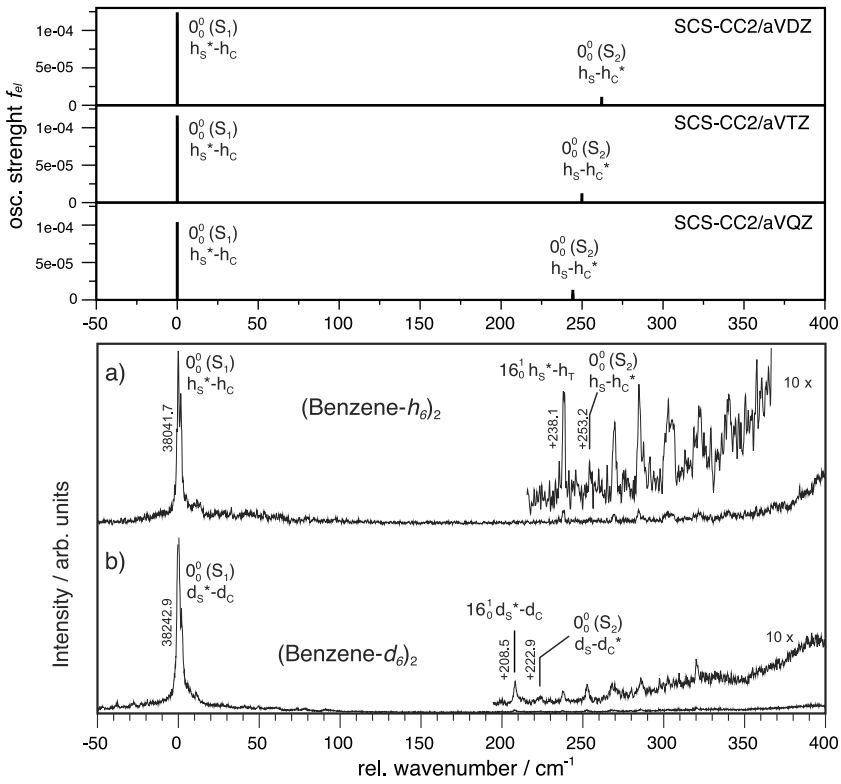

FIG. 7. Top: SCS-CC2 calculated vertical frequencies and oscillator strengths of the $(benzene)_2$ $S_0 \rightarrow S_1/S_2$ transitions with the aVXZ (X = D,T,Q) basis sets. The calculated frequencies are shifted by about −2000 cm^{-1} to coincide with the experimental $S_1(0^0_0)$ band. Bottom: two-color resonant two-photon ionization spectra of (a) $(benzene\text{-}h_6)_2$ and (b) $(benzene\text{-}d_6)_2$. Wavenumber scales are set to zero at the respective $S_0 \rightarrow S_1$ origins; the respective wavenumbers are given next to the 0^0_0 bands. The medium weak bands at 0^0_0+238.1 cm^{-1} in (a) and at 0^0_0+208.5 cm^{-1} in (b) are assigned to the 16^1_0 (e_{2u}) out-of-plane vibrational fundamental of the "stem" Bz-h_6 or Bz-d_6 moiety. The following weak bands are attributed to the weak $S_0 \rightarrow S_2$ transition.

series of weak bands to the $S_0 \rightarrow S_2$ excitation. The observed ratio between the $S_0 \rightarrow S_1$ 0_0^0 band intensity and the integrated intensity of the weak $S_0 \rightarrow S_2$ bands agrees nicely with the SCS-CC2 relative oscillator strengths $f_{el}(S_1)$ and $f_{el}(S_2)$. The spacing between the bands is ~15 cm^{-1}, increasing to ~20 cm^{-1} for both (Bz-h_6)$_2$ *and* (Bz-d_6)$_2$. The low frequency spacing between the bands implies the participation of one or several intermolecular vibrational modes, as discussed below.

C. R2PI spectrum of imidazole · (benzene)$_2$

Figure 8(b) shows the two-color R2PI spectrum of the imidazole · (benzene)$_2$ (Im · Bz$_2$) cluster, which has recently been observed in a spectroscopic study of the imidazole · benzene dimer.[37,51] The calculated structure of this cyclic trimer is shown in the inset of Figure 8. It involves a NH · · · π interaction from the imidazole to benzene-1 followed by sequential CH · · · π interactions from benzene-1 to benzene-2 and then from benzene-2 back to imidazole. The (Bz)$_2$ moiety contained within the Im · Bz$_2$ trimer is roughly T-shaped, with Bz-1 acting as the stem and Bz-2 as the cap molecule. The additional interaction with imidazole tilts the stem Bz-1 along the δ angle, which is defined for the **S3a** structure of (Bz)$_2$ shown in Figure 1(c). Relative to the **S3** structure in Figure 1(b), the symmetry descent is $C_{2v} \rightarrow C_s'$, where the prime indicates that the mirror plane of the **S3a** (C_s') structure is not the same as that in the **M2** (C_s) structure.

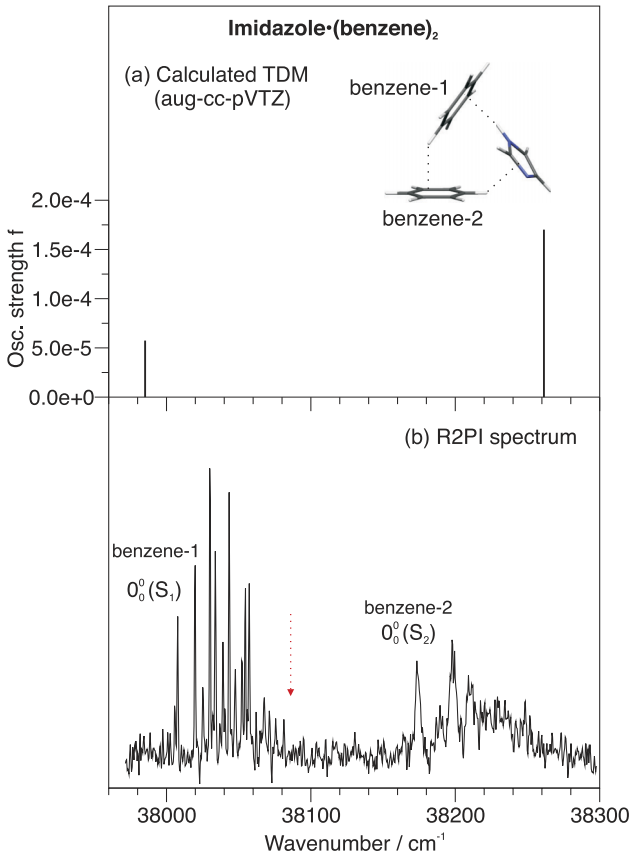

FIG. 8. (a) SCS-MP2 calculated ground-state equilibrium structure of imidazole · (benzene)$_2$ (Im · Bz$_2$) and the SCS-CC2/aVTZ calculated intensities and vertical frequencies of the S_1 and S_2 electronic excitations (shifted by −2750 cm^{-1}), see Refs. 37 and 51. (b) Two-color R2PI spectrum of imidazole · benzene$_2$ in the same region as Figure 7(a). The vibronic band groups between 38 000-38 100 cm^{-1} and 38 175-38 300 cm^{-1} correspond to the $S_0 \rightarrow S_1$ and $S_0 \rightarrow S_2$ excitations of (Bz)$_2$ within the trimer. The forbidden benzene $S_0 \rightarrow S_1$ electronic origin is indicated by a red vertical arrow.

Since the cap (or Bz-2) moiety in Im · Bz$_2$ also acts as a stem-type CH · · · π donor to imidazole, it acquires a much larger $S_0 \rightarrow S_1$ transition dipole moment than the cap-Bz in (Bz)$_2$. This is brought out by the SCS-CC2/aVTZ calculated transition intensities, which are $f_{el}(S_1) : f_{el}(S_2) = 1 : 3.0$ for the two benzene chromophores, as shown in Figure 8(a).[37] Therefore, the Im · Bz$_2$ cluster exhibits two electronic transitions corresponding to the two Bz chromophores, but with more similar intensities, as shown in Figure 8.

According to the SCS-CC2/aVTZ calculations, the $S_0 \rightarrow S_1$ and $S_0 \rightarrow S_2$ excitations of Im · Bz$_2$ correspond to simultaneous excitations of both Bz-1 and Bz-2 moieties.[37] The experimental ratio of the integrated band structure corresponding to the $S_0 \rightarrow S_1$ and $S_0 \rightarrow S_2$ transitions of imidazole · (benzene)$_2$ is $f_{el}(S_1) : f_{el}(S_2) = 1 : 2.9$, in very good agreement with the vertical SCS-CC2/aVTZ calculation, see above. Note that the 0_0^0 band of the $S_0 \rightarrow S_2$ transition of Im · Bz$_2$ has a width of 3.6 cm^{-1} (FWHM), which is considerably broader than the $0_0^0(S_1)$, which is only 0.9 cm^{-1} (FWHM) wide. This implies that the S_2 state of Im · Bz$_2$ is more strongly coupled to the S_1 state than in (Bz)$_2$.

IV. DISCUSSION

A. Appearance of forbidden vibrational transitions

As discussed in Sec. III C, the bands at 0_0^0 + 238.5 cm^{-1} in (Bz-h_6)$_2$ and at 0_0^0 + 208.5 cm^{-1} in (Bz-d_6)$_2$ correspond very closely to the S_1 state ν_{16}' frequencies of bare benzene, which are 238 cm^{-1} in benzene-h_6 and 208 cm^{-1} in benzene-d_6.[23,50] The ν_{16}' mode is degenerate (e_{2u}) and its vibronic species in the S_1 state of Bz-h_6 and Bz-d_6 is $B_{2u} \otimes e_{2u} = E_{1g}$. Therefore, the 16_0^1 fundamental transition of bare Bz-h_6 or Bz- d_6 is electric-dipole forbidden in excitation from the A_{1g} ground-state $v'' = 0$ level, as discussed above.[21–23]

The SCS-CC2 calculations in Sec. II B predict that the $S_0 \rightarrow S_1$ 0_0^0 excitation of the T-shaped **M2** dimer is associated with the stem-Bz moiety. The appearance of the 16_0^1 band in (Bz-h_6)$_2$ and (Bz-d_6)$_2$ therefore reflects a symmetry lowering of the *stem*-Bz. The symmetry descents to energetically low-lying geometries[3,4] are from D_{6h} in bare Bz to C_{2v} in **S3**, to C_s in **M2**, or to C_s' in **S3a**, see Figure 1. The $D_{6h} \rightarrow C_{2v}$ descent splits the e_{2u} vibration into a_2 and b_2 components.[52] Since the $S_0 \rightarrow S_1$ TDM transforms as a_1 in C_{2v}, neither component of ν_{16}' becomes allowed. The $D_{6h} \rightarrow C_s$ descent splits e_{2u} into $a'' + a''$; the electronic TDM transforms as a' (see Figure 5), and again, neither component is allowed. The $D_{6h} \rightarrow C_s'$ descent to **S3a** splits e_{2u} into $a' + a''$ and the electronic TDM transforms as a', which makes the ν_{16a}' component electric-dipole-allowed.

Conversely, the appearance of the 16_0^1 fundamental in the $S_0 \rightarrow S_1$ spectrum implies the existence of S_0 state levels of (Bz-h_6)$_2$ and (Bz-d_6)$_2$ that (1) have a rigid-molecule symmetry equivalent to C_s' and (2) are populated at the T = 3–5 K

temperature of the supersonic-jet expansion. These levels must be a subset of the low-lying VRT states of $(Bz)_2$ with an average geometry that lies close to **S3a**. A permutation/inversion group-theoretical treatment of the low-lying VRT states of non-rigid $(Bz)_2$ is given in Ref. 4. In summary, the $D_{6h} \rightarrow C_s$ symmetry lowering for ground-state VRT levels whose geometries are close to the **M2** minimum of the S_0 surface renders the 0_0^0 (S_1) band of $(Bz)_2$ allowed. The alternative $D_{6h} \rightarrow C_s'$ symmetry lowering to different ground-state VRT levels with average geometries close to the **S3a** saddle point renders the 16_0^1 transition allowed.

B. The $S_0 \rightarrow S_2$ electronic transition

Starting at $0_0^0 + 223$ cm^{-1} in $(Bz\text{-}d_6)_2$ and at +253 cm^{-1} in $(Bz\text{-}h_6)_2$, six weak bands appear further towards the blue. Since Bz-d_6 and Bz-h_6 have no low-lying vibrations other than ν_{16}, we assign these bands to the $S_0 \rightarrow S_2$ electronic transition. This confirms the prediction of the SCS-CC2 calculations that (1) the S_1 and S_2 electronic excited states of $(Bz)_2$ are spaced by approximately 250 cm^{-1} and (2) the $S_0 \rightarrow S_2$ transition is about 10 times weaker than that to the S_1 state. The experimental $S_1 : S_2$ intensity ratio of the 0_0^0 bands is about 10:1. The observed splitting for $(Bz)_2$ is 253 cm^{-1} and that of $(Bz\text{-}d_6)_2$ is 223 cm^{-1}. The experimental values include differential zero-point energy effects, i.e., the difference between the excited-state and ground-state total zero-point vibrational energies.

The intensities and spacings of the bands associated with the $S_0 \rightarrow S_2$ electronic transition are similar to the bands that are associated with the $S_1(6_0^1)$ intramolecular excitation of $(Bz)_2$. The ground-state van der Waals vibrational modes of $(Bz)_2$ have been extensively discussed by Felker and coworkers[14] and have been calculated by Hobza and co-workers.[25] Our preliminary assignments of the $S_0 \rightarrow S_2$ bands are shown in Figure 9. The intermolecular vibrations involved are probably the totally symmetric modes ω', σ', and χ', based on ground-state normal mode calculations at the SCS-CC2/aVDZ level. The calculated and experimental frequencies are given in Table II.

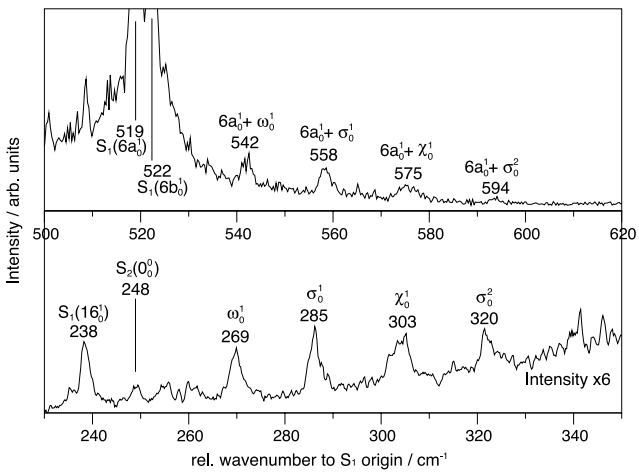

FIG. 9. Two-color R2PI spectrum of (benzene-h_6)$_2$ in the $S_1(6_0^1)$ region (top) and in the $S_2(0_0^0)$ region (bottom), with tentative intermolecular vibrational assignments. The wavenumber scales are relative to the $(Bz)_2$ S_1 origin at 38 041.7 cm^{-1}.

TABLE II. Benzene dimer SCS-MP2/aug-cc-pVTZ S_0 state calculated and experimental intermolecular vibrational frequencies in the $S_1(6_0^1)$ and $S_2(0_0^0)$ regions (in cm^{-1}).

Mode	Label	S_0, calc.	$S_1(6_0^1)$, expt.	$S_2(0_0^0)$, expt.
Twist	θ	10.1		
Tilting	δ	14.3		
Tipping	ω	30.7	23	21
Stretch	σ	59.4	39	37
Shear	χ	68.1	56	55
Buckle	β	68.2		

C. Geometry dependence of the $S_0 \rightarrow S_1$ and $S_0 \rightarrow S_2$ electronic oscillator strengths

The SCS-CC2 calculations and Figures 2 and 6 show that the electronic oscillator strengths $f_{el}(S_1)$ and $f_{el}(S_2)$ depend on the $(Bz)_2$ structure. Figure 10 generalizes these findings by showing the S_0, S_1, and S_2 state SCS-CC2 electronic energies at the energetically low-lying stationary points **M2**, **S3**, **S3a**, **M1**, and **S8** that have been previously localized on the S_0 state CCSD(T) potential energy surface.[3,4] As in Figure 6, the calculated $f_{el}(S_1)/f_{el}(S_2)$ oscillator strengths are indicated by red/blue dots with radii that are proportional to the f_{el} values.

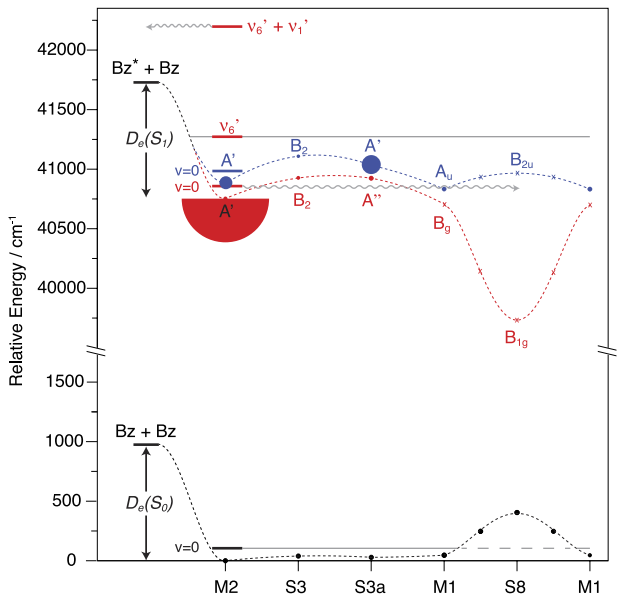

FIG. 10. SCS-CC2/aVTZ calculated vertical excitation energies and oscillator strengths f_{el} of the $S_0 \rightarrow S_1$ (red) and $S_0 \rightarrow S_2$ (blue) transitions for different T-shaped and π-stacked conformers of (benzene)$_2$ (for the conformer abbreviations see Fig. 1). The calculated energies are connected to indicate qualitative features of the S_0 (black), S_1 (red), and S_2 (blue) potential energy surfaces. The electronic oscillator strengths f_{el} are indicated by dot radii as in Figure 6, points labeled "x" mean that $f_{el} < 10^{-6}$. The largest $f_{el}(S_1) = 1.2 \times 10^{-4}$ for **M2** is halved for clarity. The S_0 state energies of the **M2**, **S3**, **S3a**, **M1**, and **S8** conformers are from Ref. 4. The energy and f_{el} values for the point between **M1** and **S8** are from a SCS-CC2/aVTZ calculation. The S_0 state binding energy $D_e(S_0)$ is from Ref. 4; the S_1 and S_2 binding energies D_e are discussed in the text.

The ground- and excited-state dissociation energies for the $(Bz)_2 \rightarrow Bz + Bz$ and $(Bz)_2^* \rightarrow Bz + Bz^*$ processes are indicated at the left side of Figure 10. For the S_0 state of the **M2** structure, van der Avoird *et al.* have calculated a CCSD(T) binding energy of $D_e = 975$ cm^{-1} and a dissociation energy of $D_0 = 870$ cm^{-1}.[4] Since the $S_0 \rightarrow S_1$ electronic origin of **M2** lies 44 cm^{-1} below the (forbidden) $S_0 \rightarrow S_1$ electronic origin of benzene at 38 086 cm^{-1}, the S_1 state dissociation energy of **M2** is 44 cm^{-1} larger than the ground-state value, yielding $D_0(S_1) = 914$ cm^{-1} and $D_e(S_1) \sim 1020$ cm^{-1} for the S_1 state local minimum corresponding to **M2**, see Figure 10.

Overall, the largest oscillator strength is $f_{el}(S_1)$ of the **M2** structure; only half of the dot is shown for clarity in Figure 10. As discussed above, the $f_{el}(S_2)$ at the **M2** geometry is ~10 times smaller than $f_{el}(S_1)$, in agreement with experiment. The decrease of ω towards zero decreases both $f_{el}(S_1)$ and $f_{el}(S_2)$, as shown in Figure 6. This renders low-lying S_0 state VRT levels that are associated with the **S3** structure difficult to observe by electronic spectroscopy.

For the **S3a** geometry, Figure 10 shows that $f_{el}(S_2)$ is ~10× larger than $f_{el}(S_1)$ and also twice that of $f_{el}(S_2)$ at **M2**. The calculated $S_0 \rightarrow S_2$ transition energy is close to the $S_0 \rightarrow S_2$ transition of **M2**. This implies that transitions from ground-state VRT levels with average geometries close to **S3a** might appear intermingled with the $S_0 \rightarrow S_2$ transition of **M2**. This may explain part of the band structure observed in the S_2 region of Figures 7(a) and 7(b).

Continuing along the abscissa of Figure 10 leads to the parallel-displaced **M1** structure, see Figure 1(d), which is a ground-state local minimum.[3,4] Its $S_0 \rightarrow S_1$ transition is $A_g \rightarrow B_g$ in C_{2h} and is electric-dipole forbidden.[27–30] However, the $S_0 \rightarrow S_2$ transition of **M1** is weakly allowed, and we discuss this further below.

Starting at the S_1 state barrier between **S3** and **S3a**, the S_1 and S_2 potentials in Figure 10 slope downwards towards **M1**. The S_1 energy decreases by ~1100 cm^{-1} upon reaching the minimum at the stacked-parallel **S8** geometry, which is shown in Figure 1(e). This S_1 state well corresponds to the B_{1g} excimer state of $(Bz)_2$, which has been extensively treated by calculations at different levels of theory.[27–31] Note that the interplanar distance of **S8**—at which the vertical electronic excitations are calculated—is $R \sim 3.7$ Å, longer than the optimum distance $R_e = 3.05$ Å in the $S_1(B_{1g})$ state, thus the true B_{1g} minimum is much deeper than shown in Figure 10.[27–32] Several theory groups have studied the $^1B_{1g}$ and $^1B_{2u}$ excimer states of the **S8** and **M1** benzene dimer, usually as a function of the interplanar distance R while maintaining the D_{6h} and D_{2h} symmetries, respectively.[27–32] The calculated B_{1g} excimer well depths range between $D_e = 0.46$ eV (3570 cm^{-1})[27] and $D_e = 0.70$ eV (5650 cm^{-1})[29] at the TD-DFT level and $D_e = 0.43$ eV (3470 cm^{-1}) at the CASPT2 level.[28]

The $S_0 \rightarrow S_1$ and $S_0 \rightarrow S_2$ transitions of D_{6h}-symmetric **S8** are both electric-dipole forbidden.[27,29,31] However, at the **M1** geometry—which may be populated in the supersonic jet experiments—the symmetry lowering to C_{2h} renders the $S_0 \rightarrow S_2$ transition slightly allowed. The SCS-CC2 calculated $f_{el}(S_2)$ is 3.40×10^{-6}, which is 35% of that at the **M2** minimum. Since the S_1 state surface at the **M1** geometry is strongly tipped towards **S8**, the $S_0 \rightarrow S_2$ transition of **M1** leads to levels that will couple to vibrations high up in the B_{1g} excimer well, see Figure 10, and the high vibrational mode density at this energy should lead to a broad and continuous band shape. The SCS-CC2 predicted $S_0 \rightarrow S_2$ transition energy **M1** lies near or below to the S_1 origin of **M2**. We propose that the $S_0 \rightarrow S_2$ absorption from **M1**-type ground-state VRT levels contributes to the weak and broad features underlying the $S_0 \rightarrow S_2$ origin in the R2PI spectrum, see Figure 7.

D. The excited-state T-shape ↔ excimer interconversion

Saigusa and co-workers have experimentally studied the formation and fluorescence of the $(Bz)_2^*$ excimer following electronic excitation of **M2** at its 0_0^0, 6_0^1, and $6_0^1 1_0^1$ vibronic bands.[18] The corresponding S_1 state levels are shown in Figure 10 as short red horizontal bars above **M2**. When exciting at the 0_0^0 band, they observed *only* broad, red-shifted excimer fluorescence with a maximum at 32 000 cm^{-1} and interpreted this as a tunneling-induced isomerization process leading from the initial **M2** to the **S8** excimer geometry.[18] This process is indicated by a horizontal oscillatory line in Figure 10. Rocha-Rinza *et al.* have calculated the S_1 state PES along the two coordinates R and δ at the CASPT2 level with an atomic natural orbital basis set and found a 160 cm^{-1} (0.02 eV) barrier along the **S3** → **S3a** → **M1** S_1 state path,[28] in qualitative agreement with Figure 10. Figure 10 indicates that the tunneling from the **M2** $v' = 0$ level produces the S_1 state excimer in highly excited vibrations that access geometries ranging from **S8** to **M1** and **S3a**; the resulting breaking of the D_{6h} symmetry of **S8** gives rise to weakly allowed fluorescence, as observed by Saigusa and co-workers.[18] The high density of vibrational states in the B_{1g} excimer well renders back-tunneling to states near the T-shaped $v' = 0$ level exceedingly improbable, in agreement with experiment.[18]

Interestingly, Saigusa and co-workers observed *both* resonance fluorescence from the T-shaped dimer and excimer fluorescence when exciting the 6_0^1 (S_1) band and interpreted this in terms of an excited-state equilibrium between T-shaped and excimer geometries.[18] Figure 10 shows that—in contrast to the $v' = 0$ level—the ν_6' level lies well above the S_1 state barrier. While the vibrational level density corresponding to **M2** is much larger at the ν_6' vibrational energy than at the $v' = 0$ level, the mode density of the excimer structures also increases, so it is not immediately obvious that the T-shape ↔ excimer equilibrium is strongly shifted toward the T-shaped structure. However, Figure 10 shows that the T-shaped structures have much larger oscillator strengths for fluorescence emission to S_0 than the excimer-type structures. This strongly biases the probability for *observing* resonance fluorescence in favor of the T-shaped structures. When exciting at the $6_0^1 1_0^1$ band, Saigusa and co-workers observed only Bz^* monomer fluorescence and interpreted this as dimer dissociation being fast relative to excimer formation and fluorescence.[18] This is in agreement with the position of the $\nu_6' + \nu_1'$ level, which lies above the dissociation limit to $Bz + Bz^*$. The dissociation process is schematically indicated shown in Figure 10.

In summary, the combination of the S_1 and S_2 state SCS-CC2 potential energy surfaces with the CCSD(T) ground-state

binding and dissociation energies of van der Avoird *et al.*[4] and other spectroscopic data given in Figure 10 allow to confirm and interpret the conjecture of several groups that the excited T-shaped $(Bz)_2$ dimer is only a local on the S_1 state surface.[8,9,18] The S_1 and S_2 state surfaces are also in agreement and are consistent with the vibration-dependent fluorescence excitation/emission results of Saigusa and co-workers.[18]

V. CONCLUSIONS

Vibronically resolved mass-selective electronic spectra of $(Bz\text{-}h_6)_2$ and its isotopomer $(Bz\text{-}d_6)_2$ are presented that show the well-known $S_0 \rightarrow S_1$ transition as well as the $S_0 \rightarrow S_2$ transition, which has not been reported before. The $S_0 \rightarrow S_2$ transition is shifted by +253 cm^{-1} for $(Bz\text{-}h_6)_2$ and by +223 cm^{-1} for $(Bz\text{-}d_6)_2$ relative to the corresponding $S_0 \rightarrow S_1$ origin.

The agreement with SCS-CC2/aug-cc-pVQZ vertical excitation energies and corresponding oscillator strengths is excellent. We show that the oscillator strengths are strongly geometry dependent: at the T-shaped C_{2v} level, the oscillator strengths of both transitions were nearly zero, whereas at C_s symmetry, a $S_1 : S_2$ ratio of roughly 10:1 was predicted by the calculations and confirmed by experiment. This conclusively shows that the ~2 cm^{-1} splitting on the electronic origin of the S_1 state of $(benzene)_2$ does not arise from an excitonic interaction.[10,12] The S_1/S_2 splitting is dominated by the structural inequivalence of the two Bz chromophores.[13–15]

The R2PI spectrum of the trimer imidazole · $(benzene)_2$ is presented in comparison: the two benzene units within this trimer complex form a structure similar to the $(benzene)_2$, although the stem benzene is tipped sideways, similar to **S3a** due to the interaction with the imidazole moiety. The R2PI spectra of imidazole · $(benzene)_2$ confirm the strong geometry dependence of the $f_{el}(S_1)$ and $f_{el}(S_2)$ oscillator strengths: the $S_0 \rightarrow S_2$ transition is much stronger in imidazole · $(benzene)_2$ than in $(benzene)_2$ because the benzene moieties are fixed at a low-symmetry geometry and are strongly tilted compared to $(benzene)_2$. The $S_0 \rightarrow S_1$/ S_2 electronic origin frequencies of imidazole · $(benzene)_2$ lie very close to those of $(Bz)_2$, thereby confirming the interpretation of the $(Bz)_2$ spectrum. The calculated $f_{el}(S_1)$ and $f_{el}(S_2)$ oscillator strengths of imidazole · $(benzene)_2$ agree well with the observed spectrum.

Vertical excitation energies of the S_1 and S_2 states were calculated at five ground-state stationary-point geometries ranging from the T-shaped **M2**, **S3**, and **S3a** structures to the stacked **M1** and **S8** geometries. The excited-state potentials constructed from these energies agree with the proposition of earlier workers[8,9,18] that the $S_0 \rightarrow S_1$ excitation of $(benzene)_2$ leads to a T-shaped local minimum that rapidly rearranges into a vibrationally excited excimer geometry, and that ionization takes place from the B_{1g} excimer state. Since the 0_0^0 band has a width of ~1.3 cm^{-1},[8,9,12–15,18] the lifetime for tunneling out of this minimum is ≥7 ps, but it has never been directly measured.

We also interpret the state-specific fluorescence properties[18] of the $v' = 0$, ν_6' and $\nu_6' + \nu_1'$ levels of $(Bz)_2^*$ in terms of the S_1/S_2 potential energy and transition-dipole moment surfaces. The ν_6' level of $(Bz)_2$ is embedded in a huge background density of vibrations of the B_{1g} excimer minimum that lies 3000–4500 cm^{-1} lower. The dissociation of the $(Bz)_2^*$ upon excitation at the $6_0^1 1_0^1$ band[18] agrees well with our calculations.

Combining these results with previous calculations of the S_1 and S_2 excited states at the **M1** and **S8** geometries,[28–32] we show that the $S_0 \rightarrow S_1$ and $S_0 \rightarrow S_2$ transitions are optically forbidden for many ground-state structures that are populated in the jet-cooled $(Bz)_2$ ground state, specifically for VRT levels near **S3** and **M1**. The only other structure with a reasonable transition-dipole moment is the C_s' symmetric T-shaped dimer **S3a**, which has a moderately intense $S_0 \rightarrow S_2$ and a weak $S_0 \rightarrow S_1$ transition. This strong bias of the S_1 and S_2 transition-dipole moment surfaces of $(Bz)_2$ against geometries that are *not* T-shaped, such as **M1** and **S8**, is the main reason why all vibronic spectroscopic experiments on jet-cooled $(Bz)_2$ to date have indicated a T-shaped structure,[8,9,12–15,17,18] although theory predicts that the parallel-displaced **M1** structure is a local minimum.[27–32]

The electronic spectrum of jet-cooled $(Bz)_2$ can only be observed through an experimental "keyhole" that strongly favors observation of the T-shaped geometry and does not allow to observe the other low-energy minima on the S_0 state surface. An analogous bias exists against the microwave spectroscopic observation[2,5–7] of VRT ground-state levels near the **M1** parallel displaced structure, because the **M1** structure has no permanent dipole moment.

ACKNOWLEDGMENTS

Financial support by the Schweizerische Nationalfonds (Project Nos. 200021-132540) is gratefully acknowledged.

[1] J. M. Steed, T. A. Dixon, and W. Klemperer, J. Chem. Phys. **70**, 4940 (1979).
[2] E. Arunan and H. S. Gutowsky, J. Chem. Phys. **98**, 4294 (1993).
[3] R. Podeszwa, R. Bukowski, and K. Szalewicz, J. Phys. Chem. A **110**, 10345 (2006).
[4] A. van der Avoird, R. Podeszwa, K. Szalewicz, C. Leforestier, R. van Harrevelt, P. R. Bunker, M. Schnell, G. von Helden, and G. Meijer, Phys. Chem. Chem. Phys. **12**, 8219 (2010).
[5] M. Schnell, U. Erlekam, P. R. Bunker, G. von Helden, J.-U. Grabow, G. Meijer, and A. van der Avoird, Angew. Chem., Int. Ed. **52**, 5180 (2013).
[6] M. Schnell, U. Erlekam, P. R. Bunker, G. von Helden, J.-U. Grabow, G. Meijer, and A. van der Avoird, Phys. Chem. Chem. Phys. **15**, 10207 (2013).
[7] M. Schnell, P. R. Bunker, G. von Helden, J.-U. Grabow, G. Meijer, and A. van der Avoird, J. Phys. Chem. A **117**, 13775 (2013).
[8] J. B. Hopkins, D. E. Powers, and R. E. Smalley, J. Phys. Chem. **85**, 3739 (1981).
[9] P. R. R. Langridge-Smith, D. V. Brumbaugh, C. A. Haynam, and D. H. Levy, J. Phys. Chem. **85**, 3742 (1981).
[10] K. O. Börnsen, H. L. Selzle, and E. W. Schlag, Z. Naturforsch., A **39**, 1225 (1984).
[11] K. S. Law, M. Schauer, and E. R. Bernstein, J. Chem. Phys. **81**, 4871 (1984).
[12] K. O. Börnsen, H. Selzle, and E. Schlag, J. Chem. Phys. **85**, 1726 (1986).
[13] B. F. Henson, G. V. Hartland, V. Venturo, R. A. Hertz, and P. Felker, Chem. Phys. Lett. **176**, 91 (1991).
[14] B. F. Henson, G. V. Hartland, V. A. Venturo, and P. M. Felker, J. Chem. Phys. **97**, 2189 (1992).
[15] V. Venturo and P. M. Felker, J. Chem. Phys. **99**, 748 (1993).
[16] V. Venturo and P. M. Felker, J. Phys. Chem. **97**, 4882 (1993).
[17] W. Scherzer, O. Krätschmar, H. L. Selzle, and E. W. Schlag, Z. Naturforsch., A **47**, 1248 (1992).
[18] T. Hirata, H. Ikeda, and H. Saigusa, J. Phys. Chem. A **103**, 1014 (1999).
[19] U. Erlekam, M. Frankowski, G. Meijer, and G. von Helden, J. Chem. Phys. **124**, 171101 (2006).
[20] P. Hobza, H. L. Selzle, and E. W. Schlag, J. Phys. Chem. **100**, 18790 (1996).
[21] J. H. Callomon, T. M. Dunn, and I. M. Mills, Philos. Trans. R. Soc., A **259**, 499 (1966).
[22] G. H. Atkinson and C. S. Parmenter, J. Mol. Spectrosc. **73**, 20 (1978).
[23] G. H. Atkinson and C. S. Parmenter, J. Mol. Spectrosc. **73**, 31 (1978).

[24]P. Hobza, H. L. Selzle, and E. W. Schlag, J. Chem. Phys. **93**, 5893 (1990).
[25]V. Špirko, O. Engkvist, P. Soldán, H. L. Selzle, E. W. Schlag, and P. Hobza, J. Chem. Phys. **111**, 572 (1999).
[26]W. Wang, M. Pitoak, and P. Hobza, ChemPhysChem **8**, 2107 (2007).
[27]J. Amicangelo, J. Phys. Chem. **109**, 9174 (2005).
[28]T. Rocha-Rinza, L. D. Vico, V. Veryazov, and B. Roos, Chem. Phys. Lett. **426**, 268 (2006).
[29]R. Huenerbein and S. Grimme, Chem. Phys. **343**, 362 (2008).
[30]T. Rocha-Rinza and O. Christiansen, Chem. Phys. Lett. **482**, 44 (2009).
[31]K. Diri and A. I. Krylov, J. Phys. Chem. A **116**, 653 (2012).
[32]M. Kolaski, C. R. Arunkumar, and K. S. Kim, J. Chem. Theory Comput. **9**, 847 (2013).
[33]E. Miliordos, E. Apra, and S. S. Xantheas, J. Phys. Chem. A. **118**, 7568 (2014).
[34]P. Ottiger, C. Pfaffen, R. Leist, H. M. Frey, S. Leutwyler, R. A. Bachorz, and W. Klopper, J. Phys. Chem. B **113**, 2937 (2009).
[35]C. Pfaffen, H. M. Frey, P. Ottiger, S. Leutwyler, R. A. Bachorz, and W. Klopper, Phys. Chem. Chem. Phys. **12**, 8208 (2010).
[36]C. Pfaffen, D. Infanger, P. Ottiger, H. M. Frey, and S. Leutwyler, Phys. Chem. Chem. Phys. **13**, 14110 (2011).
[37]M. A. Trachsel, P. Ottiger, H.-M. Frey, C. Pfaffen, A. Bihlmeier, W. Klopper, and S. Leutwyler, "Modeling the Histidine-Phenylalanine Interaction: The NH $\cdots\pi$ Hydrogen Bond of Imidazol $\cdot$ Benzene," J. Phys. Chem. B (in press).
[38]A. Hellweg, S. A. Grün, and C. Hättig, Phys. Chem. Chem. Phys. **10**, 4119 (2008).
[39]A. Hellweg, J. Chem. Phys. **134**, 064103 (2010).
[40]N. Winter, N. K. Graf, S. Leutwyler, and C. Hättig, Phys. Chem. Chem. Phys. **15**, 6623 (2013).
[41]C. Hättig and F. Weigend, J. Chem. Phys. **113**, 5154 (2000).
[42]S. Grimme, J. Chem. Phys. **118**, 9095 (2003).
[43]C. Hättig, J. Chem. Phys. **118**, 7751 (2003).
[44]See supplementary material at http://dx.doi.org/10.1063/1.4922608 for the Cartesian coordinates.
[45]TURBOMOLE V6.3 2011, a development of Universität Karlsruhe (TH) and Forschungszentrum Karlsruhe GmbH, TURBOMOLE GmbH, 1989-2007, see http://www.turbomole.com.
[46]R. J. Gord, A. W. Garrett, R. E. Brand, and T. S. Zwier, Chem. Phys. Lett. **171**, 443 (1990).
[47]A. J. Gotch and T. S. Zwier, J. Chem. Phys. **96**, 3388 (1992).
[48]A. Garrett, D. L. Severance, and T. Zwier, J. Chem. Phys. **96**, 7245 (1992).
[49]A. J. Gotch and T. S. Zwier, J. Chem. Phys. **93**, 6977 (1990).
[50]F. M. Garforth and C. K. Ingold, J. Chem. Soc. **1948**, 440.
[51]S. Ahnen, A.-S. Hehn, K. D. Vogiatzis, M. A. Trachsel, S. Leutwyler, and W. Klopper, Chem. Phys. **441**, 17 (2014).
[52]H. Ibach, *Physics of Surfaces and Interfaces* (Springer-Verlag, Berlin, Heidelberg, 2006).